

https://doi.org/10.1070/QEL17484

Laser bleaching of tattoos: a new approach

A.G. Shubnyy, V.S. Zhigarkov, V.I. Yusupov, A.P. Sviridov

Abstract. **The dynamics of the formation and relaxation of microbubbles in a polyacrylamide phantom of tattooed skin under the action of a series of laser pulses with 15-ns duration is studied. It is shown that the growth of microbubbles occurs within a few milliseconds, and their lifetime varies from several seconds to several hours, depending on the water content in the phantom and the fluence (energy density) of laser radiation. It is found that the multipulse laser exposure regime, in comparison with the single-pulse regime, reduces the laser radiation fluence and significantly increases the degree of phantom bleaching. A region of parameters (number of pulses, fluence), in which a high concentration of undesirable (blocking laser radiation) long-lived bubbles does not form, while the bleaching effect reaches its maximum, is found. A mechanism for effective tattoo removal, based on selective thermolysis under conditions of a decrease in the thermal conductivity of the medium in the immediate vicinity of pigmented particles due to the formation of microbubbles, is proposed.**

Keywords: *tattoo removal, phantoms of tattooed skin, optical bleaching, multipulse regime, bleaching mechanism, microbubble effect.*

1. Introduction

Tattooing on a human body is one of the most ancient arts [1]. In modern youth culture, tattoos are extremely popular as a means of individuality expression. However, a person's views, values and tastes may change over time, so there is a great need for effective tattoo removal techniques. It is known that in the United States, the market for tattoo removal is ten times larger than the market for their application. The 'gold standard' for tattoo removal is currently laser-based skin treatment. The advantage of laser radiation is the ability to selectively destroy the dye ink, leaving the surrounding tissues virtually intact [2]. A significant limitation of the use of lasers for tattoo removal is the need to repeat the procedure, since a single irradiation of the tattooed skin is usually insufficient. The desired aesthetic effect is reached only after several sessions, which are repeated approximately once a month [3]. At generally accepted fluence values (laser radiation energy per unit area) up to 10 J cm^{-2} [3], exposure to a single laser pulse leads to the formation of long-lived gas bubbles in the skin dermis, blocking the penetration of light into the deeper skin layers. As the laser fluence increases, the number of gas bubbles increases rapidly; however, the probability of various complications also increases [3]. Ink particles are structures with a size of 30–300 nm. They contain oxides of various metals (aluminium, iron, copper, titanium, etc.). The exception is black ink which primarily uses carbon black. The ink injected under the skin also contains a water-based or alcohol-based solvent, glycerol, various additives to maintain a stable colloidal solution, thickeners, etc. [4].

For tattoo particles with a size of 100–300 nm, the thermal relaxation time is ~10 ns [5]. Therefore, when the laser pulse duration is less than 10 ns, the energy is localised mainly in the particles themselves [6], which leads to effective destruction of the absorber [7]. For this reason, nanosecond lasers are actively used for tattoo removal [5–7].

Recently, in addition to nanosecond pulses, picosecond laser pulses have been widely used in practice and experimental research [8–11]. This increases the efficiency of destruction of the smallest ink particles, the thermal relaxation time of which lies in the sub-nanosecond range. In work [12], it was shown on samples of cotton fabric and pig skin that irradiation with femtosecond pulses can effectively and without damage clean those samples of black ink deposited on their back side, whereas a nanosecond laser does not produce such an effect. On the other hand, femtosecond lasers are much more expensive than those that are traditionally used today.

In addition to the pulse duration, the efficiency of laser bleaching of tattooed skin is affected by the radiation wavelength, the number of pulses per procedure, and the interval between procedures. Thus, the wavelengths of 694 and 755 nm are most suitable for green, black, blue, and purple tattoo colours, while the wavelength of 532 nm is most suitable for red, orange, and yellow [7]. As for the number of pulses, they are usually limited to just one, since the effect of skin 'bleaching' occurs immediately after irradiation due to the formation of long-lived bubbles [13]. The presence of bubbles makes the medium highly scattering, so that subsequent pulses prove to be ineffective [13].

Modern tattoo removal protocols allow multiple passages of single pulses over the same area of tattooed skin during a single session with an interval of 20 minutes, during which the number of gas bubbles is significantly reduced [13] (R20 method). To accelerate the release of gases, special creams are additionally used [14, 15] (R0 method).

Another approach currently being developed to increase the efficiency of laser tattoo removal by eliminating the resulting microbubbles is the use of acoustic pulse generators [16]. For example, a Rapid Acoustic Pulse (RAP) device (SkinCare

A.G. Shubnyy, V.S. Zhigarkov, V.I. Yusupov, A.P. Sviridov Institute of Photonic Technologies, Federal Research Centre 'Crystallography and Photonics', Russian Academy of Sciences, ul. Pionerskaya 2, 108840 Moscow, Troitsk, Russia; e-mail: sviridoa@gmail.com

Received 19 November 2020
Kvantovaya Elektronika **51** (1) 8–16 (2021)
Translated by M.A. Monastyrskiy

Physicians, Chestnut Hill, USA) generates short (100–200 ns) shock waves with a rate of 100 Hz. The removal of microbubbles under the impact of a shock wave occurs as a result of their fragmentation and strong compression [16].

Although laser tattoo removal continues to be the 'gold standard', in fact, within the existing approaches, the limit of its effectiveness has been reached. We believe that a further increase in the efficiency and safety of laser tattoo removal is due to the well-known accumulation effect [17] when the skin is exposed to a series of laser pulses with a fluence below the bleaching threshold for a single pulse.

The purpose of this work is to establish regularities in laser bleaching of a tattooed skin phantom and determine the parameters (the number of irradiations, laser fluence) that provide the greatest effect of ink bleaching while minimising the laser radiation fluence.

2. Materials and methods

2.1. Dye

In our work, we used Fuschia (pink) tattoo ink from Intenze (USA), which gained widespread acceptance due to its variety of palette and reliable quality. Fuschia ink contains rhodamine (C.I. 45170: 2), TiO_2 nanoparticles, distilled water, alcohol and anti-inflammatory additives. Characteristic ink particle sizes and elemental composition were determined using a PHENOM ProX scanning electron microscope (SEM) (Phenom World, Netherlands) equipped with an EDX analyser. The SEM image (Fig. 1a) clearly shows rounded particles measuring 100–350 nm. According to EDX analysis, the basic elemental composition of the dye is oxygen (69%) and titanium (26%).

For further characterisation of the Fuschia dye, its optical properties were determined, namely, the Raman spectrum (RS), absorption and photoluminescence spectra. The Raman spectrum (Fig. 1b) was measured on a dried ink sample deposited on a silicate glass substrate. When measuring the absorption spectra (Fig. 1c) and photoluminescence (Fig. 1d), a rectangular 1 mm thick cell with an aqueous solution of tattoo ink at a mass concentration of ~0.001% was used. Photoluminescence was excited by continuous radiation from a 100-mW diode laser with a wavelength of 405 nm. The measurements were performed using a Cary 50 spectrophotometer (Varian, USA), a QE65000 spectrometer (Ocean Optics, USA), and a Raman spectrometer (Nicolet Almega XP, USA).

In the Raman spectrum (Fig. 1b), the peaks characteristic of rhodamine and TiO_2 nanoparticles are observed in the region of 1200–1600 and 400–600 cm^{-1}, respectively. In the absorption spectrum, in addition to intense bands in the short-wavelength range, there is a broad band in the region of 500– 600 nm. For the luminescence spectrum of the Fuschia dye, a distinctive feature is the presence of two broad bands with maxima at 500 and 610 nm.

2.2. Tattooed skin phantom

Human skin consists mainly of water (50%–70%), glucose, glycogen, polysaccharides, and proteins (in collagen fibres).

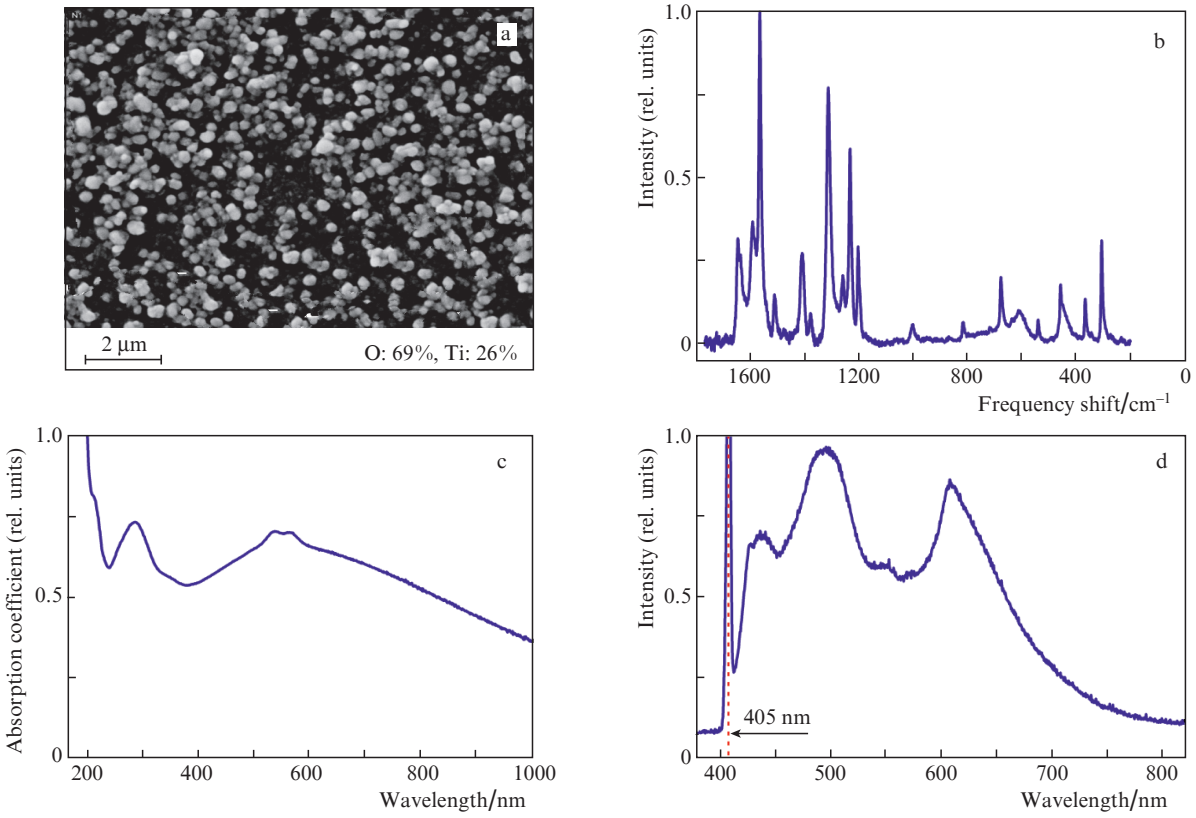

Figure 1. Characteristics of the Fuschia ink (Intenze, USA): (a) SEM image of microparticles (the elemental composition determined by EDX analysis is shown); (b) Raman spectrum of ink deposited on a silicate glass substrate; (c) absorption spectrum of an aqueous solution of tattoo ink; (d) photoluminescence spectrum of an aqueous ink solution when excited by continuous laser radiation with $\lambda = 405$ nm.

Living cells of epidermis are rich in glucation, melanin, carotenoid pigments, ascorbic acid, and mineral salts [18].

To imitate the chemical composition and physical properties of the skin dermis, we developed a composite material consisting mainly of polyacrylamide hydrogel and collagen [19]. It should be noted that earlier we used polyacrylamide hydrogel in the manufacture of optical and thermophysical equivalents of cartilaginous tissues and equipment for calibration of laser medical devices [20]. For hydrogel synthesis, acrylamide and bisacrylamide were used in a 4:1 ratio. The degree of crosslinking (the ratio of the mass of the crosslinked polymer to the total mass of the studied sample) was set by the fraction of ammonium persulfate added as an initiator of polymerisation [20]. In our case, the degree of crosslinking of the samples was 1:19, which significantly determined the scattering coefficient of the biological tissue phantom and, to a certain extent, its mechanical properties, in particular its elasticity [20]. At a crosslinking ratio of 1:19, a polyacrylamide hydrogel sample with a thickness of about 1 mm is highly elastic and transparent.

To prepare a skin dermis phantom, an aqueous solution of acrylamide and bisacrylamide monomers was poured into the space between two cover glasses located at a distance of 170 μm from each other, and ammonium persulfate was added there, initiating polymerisation and crosslinking. As a result of polymerisation, homogeneous films with a size of $\sim 25 \times 25$ mm were formed. The sides of the cover glasses were covered with molten paraffin, which protected the phantom from drying out during long-term storage. Figure 2 shows a schematic image of a tattooed skin phantom which is a dermal phantom containing ink, its photograph, and transmission spectra with and without dye. The addition of Fuschia dye reduces the transmission of light over the entire recorded wavelength range, with a maximum effect in the region of 500–600 nm.

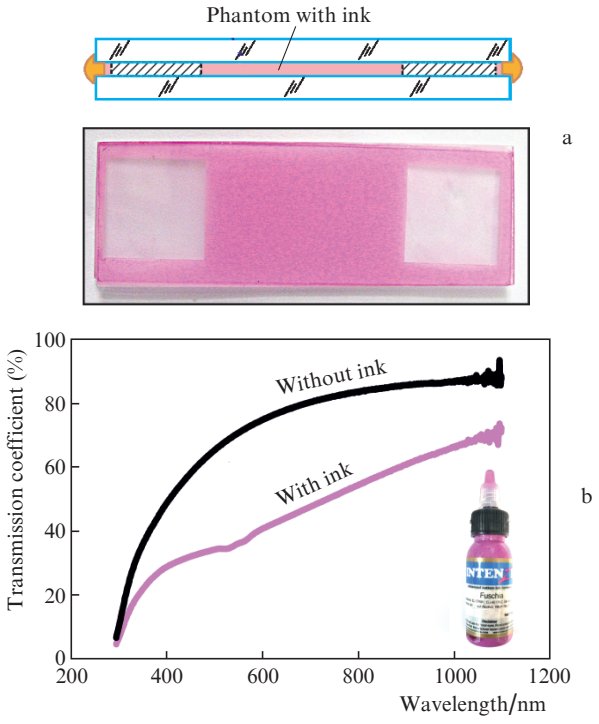

Figure 2. Characteristics of a tattooed skin phantom: (a) schematic image of the phantom with tattoo ink used in the work (cross-section and its photograph from above); (b) transmission spectrum of the phantom without ink and with Fuschia ink.

In a number of experiments, the concentration of water in the samples was varied. To do this, the upper cover glass was removed, and a frame was installed instead, holding the edges of the film with an initial water content of 70%. The sample was gradually dried in air at room temperature, which was controlled by weighing. When the required water content was reached, the sample was again covered with glass, and the side gaps between the glasses were sealed with paraffin. Although the physical thickness of the sample decreased, measurements showed that its optical density determined by the absorption of light by pigments and scattering on particles remained virtually unchanged.

2.3. Experimental setup

For irradiation of skin phantoms and real-time recording of changes in optical properties in the area of laser exposure, an experimental setup was used, the scheme of which is shown in Fig. 3.The setup is based on a 'power' Nd:YAG laser (LOTIS T11, Belarus) (*1*) with a radiation wavelength of $\lambda = 532$ nm and a pulse duration of $\tau = 15$ ns. The laser made it possible to operate in the single-pulse regime. The laser radiation power was regulated by a polarising attenuator (*2*) and controlled using a meter (S310C, Thorlabs, USA).

After passing the attenuator, the radiation was focused by a lens (*3*) and directed to a diaphragm (*4*) with a diameter of 0.3 mm. An image of the diaphragm was formed on the sample surface by lens *5*. The objects of research were phantoms of tattooed skin enclosed between cover glasses (*6*). Using a microlens ($20^{\times}$) (*7*), an enlarged image of the phantom surface was formed in the matrix plane of a digital camera (*8*). The phantom was illuminated in the transmission regime with a white light beam using a fibre optic bundle (*9*). An optical filter was installed in front of the camera, transparent in the red region and cutting off laser radiation and shorter-wavelength radiation. To study fast processes, the dynamics of the integral intensity of light scattered by the phantom was measured (Fig. 3c). In this case, the illumination was performed using a beam of a probe semiconductor laser (*10*), and direct radiation passing through the phantom was blocked by an annular shutter (*11*). Forward scattered radiation was directed to a photodiode (*13*) using lens *12*.

2.4. Processing of SEM images

To determine the concentration of TiO_2 nanoparticles and agglomerates, special processing of SEM images of irradiated and intact areas of tattooed skin phantom samples was performed. Nanoparticles containing titanium were preliminarily isolated using EDX analysis. Then, on digital SEM images in grayscale, the brightness of the B_i pixels assigned to the individual nanoparticle was estimated, and the mean $\bar{B}_i$ and standard deviation Δ were determined. Image areas with $B_i \geqslant \bar{B}_i - \Delta$ were taken as a nanoparticle. Based on the data obtained, profiles of the area occupied by TiO_2 nanoparticles were constructed, averaged over the selected image area.

2.5. Processing of optical images

The quantitative assessment of the bleaching degree of the samples was conducted as follows. We compared two frames

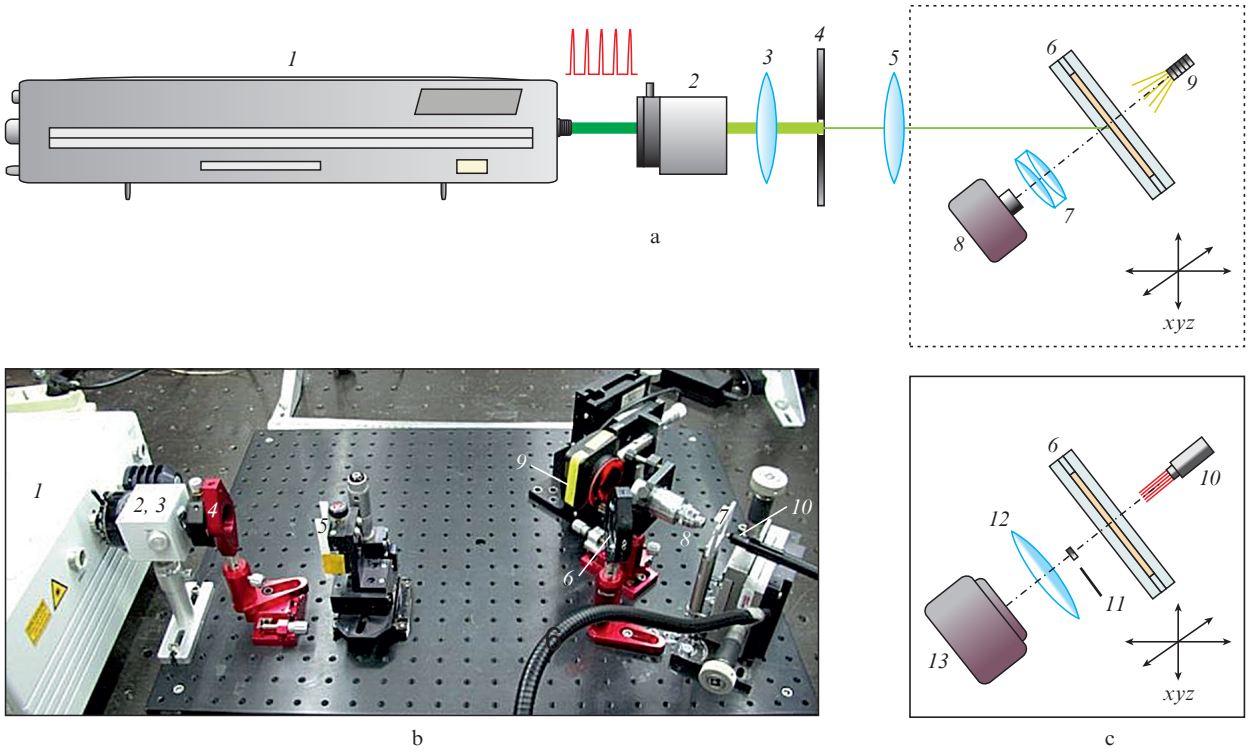

Figure 3. (a) Schematic for visualisation of processes and (b) a photograph of the main part of the experimental setup, as well as (c) a diagram of part of the setup for recording the integral intensity of scattered light [(*1*) laser; (*2*) attenuator; (*3*, *5*, *12*) lenses; (*4*) diaphragm; (*6*) glass plates with a phantom; (*7*) lens; (*8*) video camera; (*9*) illuminator; (*10*) laser illumination; (*11*) blocking shutter; (*13*) photodiode].

obtained when filming in transmitted light (diagram in Fig. 3a): before and after laser exposure. The resulting images were processed in the MATLAB environment. In the area where visual bleaching reached the greatest value, a square with a size of 50×50 pixels was selected, and the average light intensity I recorded by these pixels was calculated. Similarly, the average intensity I_0 in the same region was determined before irradiation. The degree of bleaching was found by the formula $S = 100(I - I_0)/(I_1 - I_0)$, where I_1 is the average intensity in the case of an uncoloured phantom. Thus, in the absence of bleaching, $S = 0$, and if the ink is completely decomposed, $S = 100\%$. Strictly speaking, the value of S characterises the degree of brightening in the visible spectrum range. However, since the transmitted probe light turns white after laser exposure, we can talk about bleaching based on our experimental data. Separate experimental points on the S dependences on fluence were obtained in three repeated experiments. The mean values and standard deviations are given for these experiments.

3. Experimental results

A series of experiments was conducted to identify the regularities and mechanisms of bleaching of tattooed skin under repeated laser exposure. The change in optical properties of the phantom under the action of a single laser pulse is shown in Fig. 4. It is seen that immediately after the pulsed impact, the transmitted light intensity in the laser spot decreases (Fig. 4b). A large area (*1*) with short-lived microbubbles and a single long-lived bubble (*2*) are clearly distinguished here. After one minute, bleaching is already observed in the area of laser exposure (Fig. 4c), which stably remains at the same level for a long time. Experiments have shown that short-lived microscopic bubbles disappear in a few seconds, while larger (at least 10 μm) long-lived bubbles could remain stable for up to 10 minutes or more.

The phantom study using SEM and EDX analysis has shown (Fig. 5) that a significant decrease in large TiO_2 agglomerates occurs in the irradiated region. After mathematical processing of the original SEM image (Fig. 5a), a spot with a significantly lower content of TiO_2 nanoparticles is clearly distinguished in the region of laser exposure (dashed circle in Fig. 5b). From the averaged profile of the fraction of the image area occupied by TiO_2 nanoparticles (Fig. 5c), it follows that this fraction decreases by about five times in the area of laser exposure.

Figure 6 shows the time dependences of the scattered component intensity of the probe laser beam ($\lambda = 650$ nm) passing through the tattooed skin phantoms when exposed to a single laser pulse (experiments according to the scheme in Fig. 3c). It can be seen that immediately after exposure, the intensity increases in a few milliseconds to its limiting value (Fig. 6a), and the dynamics of this process virtually does not depend on the water content in the sample. Then, as follows from Fig. 6b, the scattered light intensity remains at the same level or monotonously decreases depending on the water content in the phantom. Experiments have shown that at a water content of ~10%, the maximum level remains unchanged for at least 24 hours. If the water content is greater than or equal to 30%, the scattered light intensity decreases significantly over time.

Figure 7 shows the transmission dynamics $I(t)/I(0)$ of radiation from a probe laser (where $I(t)$ is the recorded intensity value at the time moment t, $I(0)$ is the intensity before the 'power' laser action) through the phantom after the action of a laser pulse with different fluence values [Fig. 3c, without a

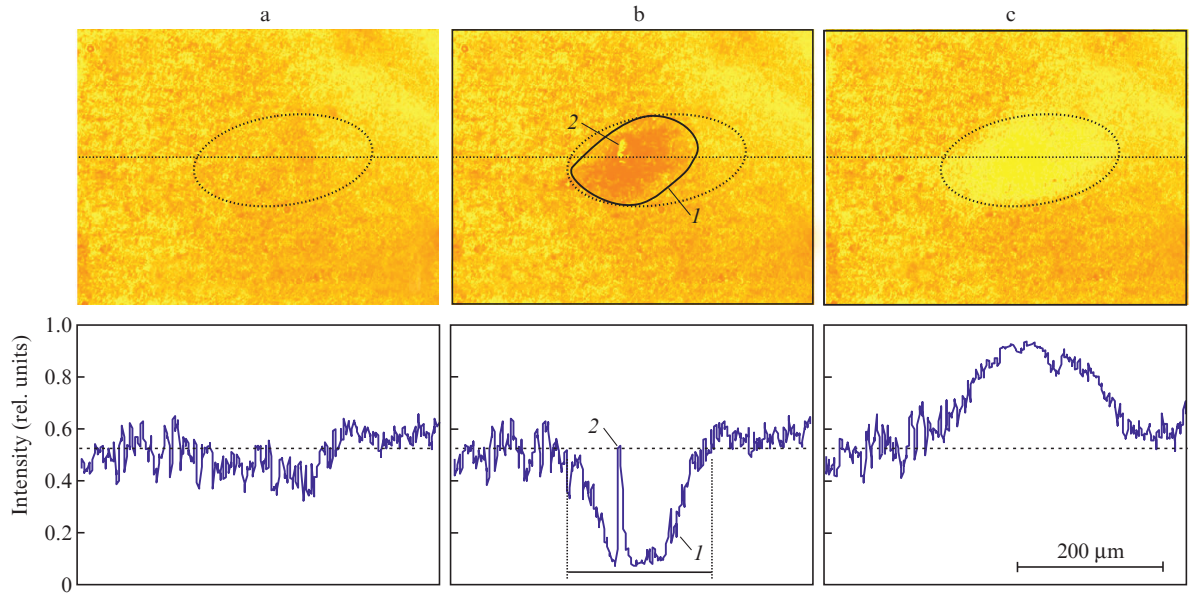

Figure 4. Bleaching of a tattooed skin phantom under the action of a single laser pulse. Selective frames of video recording when the sample is illuminated with transmitted light are shown (Fig. 3a) with the corresponding light intensity profiles along the lines passing through the spot centre (dashed horizontal lines in the frames) (a) before irradiation, (b) immediately after irradiation, and (c) after 1 min after irradiation; (*1*) region with short-lived microbubbles (solid ellipse), (*2*) long-lived bubble; the dashed ellipse outlines a bleached area in the frame. The water content in the phantom is 30%.

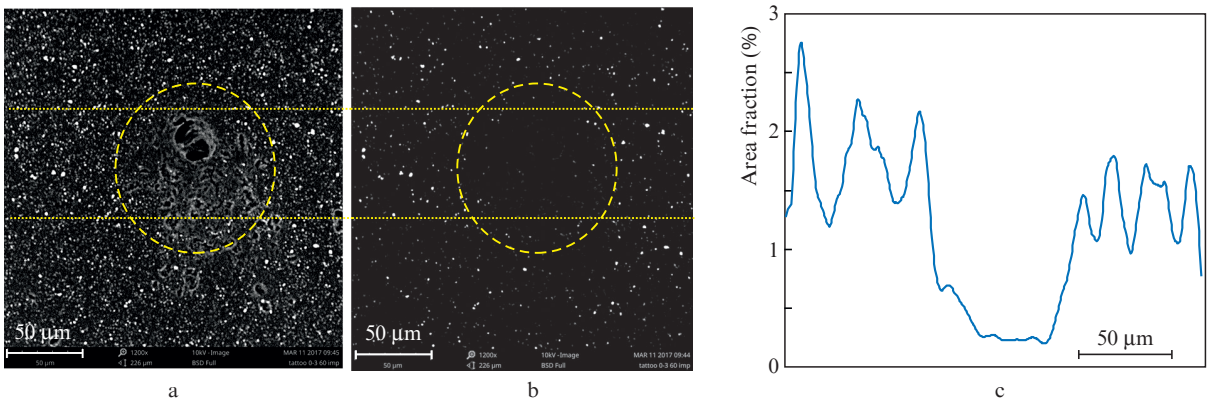

Figure 5. Laser exposure area on the tattooed skin phantom: (a) SEM image; (b) result of mathematical processing of the SEM image with the isolation of TiO_2 agglomerates; (c) profile of the image area fraction occupied by TiO_2 particles, averaged over the image area marked with dotted lines. Dashed circle marks the area with a reduced number of large agglomerates.

shutter (*11*)]. At the initial time moment, a jump in the signal is observed, caused by a 'power' nanosecond laser pulse. Immediately after this, the transmission of probe radiation through the sample decreases sharply. Then, the intensity of the transmitted probe radiation remains unchanged (for the largest fluence $\Phi = 2$ J cm^{-2}) or monotonically increases to a certain value depending on the laser pulse fluence.

Figure 8 shows the results of a study of the degree of bleaching of tattooed skin phantoms that were exposed to a series of laser pulses (1, 3, 10, 100) with a repetition rate of 1 Hz. It can be seen that for all pulse series, there are threshold fluences below which no bleaching occurs. The value of this threshold decreases as the number of pulses in the series increases. For each pulse series, when the corresponding threshold is exceeded, the bleaching degree of the sample increases with increasing fluence. Bleaching under the action of laser pulses is accompanied by the formation of bubbles. Only short-lived microbubbles are observed near the threshold. The subsequent increase in fluence leads to the appearance of fairly large long-lived bubbles, while their number gradually increases. Note that the boundary separating the regions with short-lived microbubbles (region A in Fig. 8) and long-lived bubbles (region B in Fig. 8) is described by a straight line $S[\%] = 62 - 168\Phi$ [J cm^{-2}].

As can be seen from Fig. 8, when exposed to a series of (3, 10, 100) laser pulses, a much greater bleaching degree can be achieved than when exposed to a single pulse. In this case, the maximum degree of bleaching increases with an increase in the number of pulses. For the single-pulse regime, the maximum bleaching degree was ~25%, while for a series of 3, 10, and 100 pulses, it was approximately 40%, 50%, and 60%, respectively. It should be noted that the maximum degree of

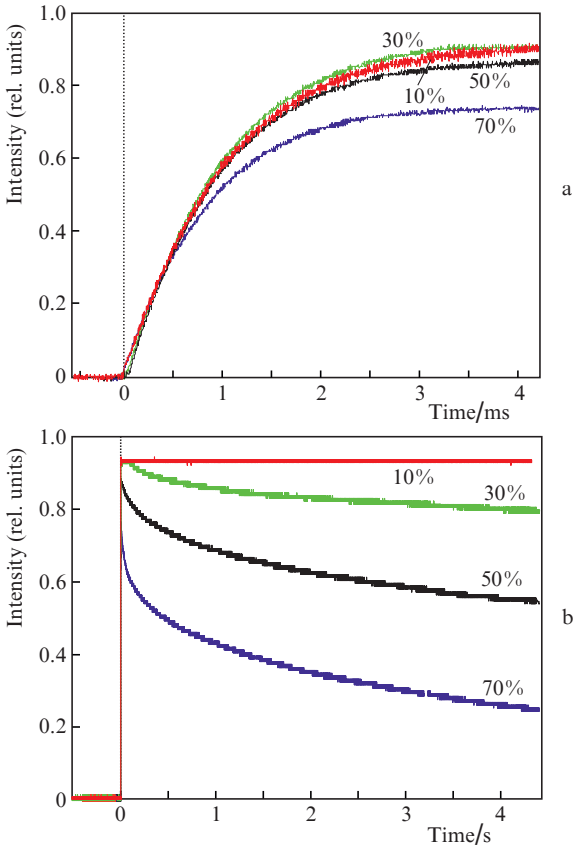

Figure 6. Dynamics of the scattered light intensity of a probe laser in millisecond (a) and second (b) time scales when tattooed skin phantoms with different water contents are irradiated by single 'power' laser pulses; fluence is 0.4 J cm^{-2}. The experiments were performed according to the scheme shown in Fig. 3c.

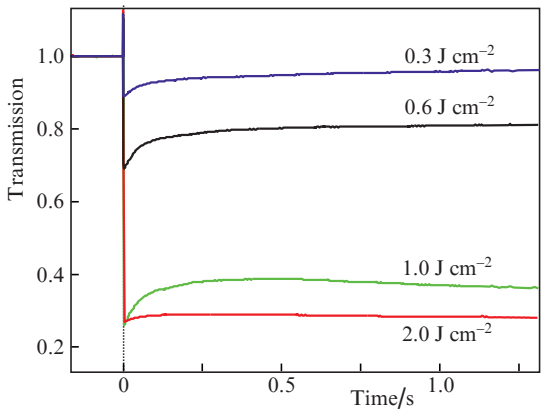

Figure 7. Transmission dynamics of probe laser radiation when tattooed skin phantoms are irradiated by single 'power' laser pulses with different fluences; the water content in the phantoms is 70%. The experiments were performed according to the scheme shown in Fig. 3 in the absence of a shutter (*11*).

bleaching for 3, 10, and 100 pulses in a series is achieved at a fluence much lower than the threshold value in the case of a single pulse. Thus, a bleaching degree of 60% can be achieved in a series of 100 pulses at $\Phi = 0.14$ J cm^{-2}, whereas in the case of a single pulse, even at $\Phi = 0.4$ J cm^{-2}, the maximum bleaching degree does not exceed 25%.

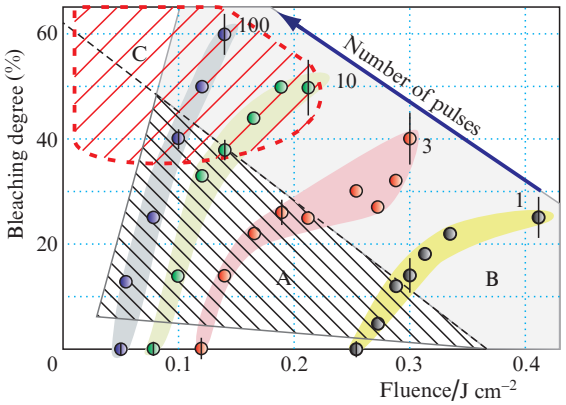

Figure 8. Dependences of the bleaching degree for a tattooed skin sample with a water content of 70% on the fluence in a single pulse and the number of pulses (1, 3, 10, and 100) in a series. The regions with short-lived microbubbles (A), long-lived bubbles (B), and a region (C) in which, in the absence of long-lived bubbles, the expected bleaching effect is maximal, are conventionally identified. The laser pulse repetition rate is 1 Hz. The measurements were conducted according to the scheme shown in Fig. 3a.

4. Discussion of the results

The results of experiments have shown that the treatment of a tattooed skin phantom with a series of laser pulses can significantly reduce the laser fluence threshold and increase the degree of bleaching compared to the single pulse regime. This indicates that as a result of the action of the first and subsequent pulses, the physicochemical properties of the phantom material change, which shifts the bleaching process towards lower fluences. Let us dwell in more detail on the facts and possible mechanisms observed in experiments.

Immediately after the pulsed action on the tattooed skin phantom, the intensity of the light passing through it in the laser spot decreases (see Fig. 4b), which is associated with the appearance of a large area with short-lived microbubbles (region *1* in Fig. 4b). The images also clearly show larger long-lived bubbles (region *2* in Fig. 4b). Within a minute after laser exposure, bleaching is observed in the focus area, which remains stable at the same level for a long time (Fig. 4c). A considerable (approximately fivefold) decrease in large TiO_2 agglomerates in the irradiated area should also be attributed to significant changes that occur after pulsed impact on the phantom (see Fig. 5).

Measurements of the intensity of the direct and scattered components of the probe radiation passing through the sample (see Figs 6 and 7), as well as observations using a microscope, made it possible to state that vapour-gas microbubbles are formed in the laser exposure zone. The size and concentration of these microbubbles reach their maximum values a few milliseconds after exposure to the laser pulse (Fig. 6a). Then the scattering of probe radiation associated with the presence of bubbles decreases.

The lifetime of laser-induced bubbles significantly depends on the water content in the phantom and reduces with its increase (Fig. 6b). With a water content of ~10%, the maximum level of the reached scattered light intensity remains unchanged for at least 24 hours, which indicates the formation of a stable porous structure in this case. At the beginning of the next laser pulse (an interval of 1 s), some of these bubbles still remain (Figs 6b and 7). Note that the dynamics of

bubble formation and relaxation also depend on the laser pulse fluence (Fig. 7).

Experiments have shown (Fig. 8) that with each subsequent laser pulse, the modification of the sample material continues. Since the dynamics of bleaching and the dynamics of microbubble accumulation are interrelated, it can be assumed that the formed bubbles play a certain role in the process of phantom bleaching.

Consider the possible mechanisms of bleaching tattooed skin phantoms under the impact of pulsed laser radiation. These include:

1. Optoacoustic fragmentation of pigmented particles.
2. Photochemical decomposition of pigment molecules.
3. Photocatalysis of chemical reactions in the presence of titanium dioxide.
4. Thermal hydrolysis of pigments.
5. Thermal decomposition of pigment molecules under pulsed laser heating.
6. Pigment etching with supercritical water.
7. Destruction of agglomerates under the action of explosive boiling of water, etc.

Currently, the most widely used models are based on non-equilibrium and inhomogeneous laser heating of tattoo dye particles, according to which the particles are destroyed as a result of the impact of shock waves generated in them and in the environment [21, 22]. Due to the inhomogeneity of heating inside the particle, significant mechanical stresses can also occur, which can destroy the particle. In principle, the combined action of shock waves and thermal inhomogeneous expansion is possible. The decrease in the threshold fluence of particle destruction by a series of laser pulses can also be explained, for example, by the process of gradual accumulation of defects and cracks to a certain critical level. However, the main thing is unclear, i.e. how the destruction of particles can lead to phantom bleaching. After all, this requires, first of all, to destroy the pigment molecules. Therefore, it is necessary to take into consideration chemical processes involving pigment molecules.

Our studies have shown that the aqueous solution of Fuschia ink remains stable under prolonged exposure to low-fluence laser radiation ($\sim$0.01 J cm^{-2}). Therefore, the single-photon decay of pigment molecules does not occur in our case. A similar conclusion can be drawn with respect to photocatalysis. It is known that titanium oxide particles can initiate various chemical reactions by generating reactive oxygen species in the water environment when exposed to visible and UV radiation [23, 24]. This is a single-photon process that is determined solely by the radiation dose.

During a laser pulse, its energy is absorbed by chromophores surrounded by water – dye nanoparticles (agglomerates), heating them. Such a nanoparticle absorbs the energy $\sigma_{abs}\Phi$ per pulse, where σ_{abs} is the absorption cross section. In the absence of heat removal, the nanoparticle temperature growth is

$$\Delta T = \frac{\sigma_{abs}\Phi}{V_{np}\rho_{np}c_{np}}, \quad (1)$$

where V_{np}, ρ_{np}, and c_{np} are volume, density, and heat capacity of the nanoparticle, respectively.

Since the nanoparticle is in a liquid, a heat flux will be released from it as a result of thermal diffusion. Therefore, the maximum temperature under the laser pulse action is reached at the nanoparticle centre, while the temperature increase will be less than (1). It is known that the shorter the pulsed irradiation time, the thinner the liquid layer heated near the nanoparticle (the temperature near the nanoparticle decreases as $1/r^3$, rather than as $1/r$, where r is the distance from the nanoparticle centre) [25]. In this case, the characteristic time for establishing the temperature profile is $\tau_T = R^2/3a$, where R is the nanoparticle radius, and a is the coefficient of thermal diffusivity of the surrounding liquid ($\sim 1.4 \times 10^{-7}$ m^2 s^{-1} for water). For nanoparticles with a radius of 100 nm, the characteristic time is $\tau_T \approx 100$ ns.

If the laser pulse duration is longer than τ_T, then during its exposure a significant part of the energy will be spent on heating the surrounding liquid. It should be taken into account the fact that if the repetition rate of laser pulses is too high, the nanoparticle will not have time to fully cool down during the time between the pulses; therefore, a gradual increase in the average temperature will be observed against the background of its pulsed heating. It is well known that the rate constant of thermal decomposition of molecules obeys the Arrhenius law. Therefore, the degree of thermal destruction can be represented as an integral:

$$\Gamma(t) = \int_0^t A \exp\left[\frac{-\Delta E}{k_B T(t')}\right] dt', \quad (2)$$

where A is the coefficient; ΔE is the activation energy; and k_B is the Boltzmann constant. Thus, the degree of destruction (the fraction of the destroyed material's volume) significantly depends on temperature as a function of time. Under laser pulsed impact, extreme conditions (high temperatures and pressures) that occur for a certain period of time in the immediate vicinity of the absorbing particle will facilitate the hydrolysis of organic molecules by superheated water or vapour. It is impossible to exclude the possibility of the formation of supercritical water (critical parameters T_c = 646.9 K, P_c = 22.06 MPa) [26], which, as is well known, interacts very actively with all organic compounds and can cause their rapid destruction [27]. Note that to test specific mechanisms of thermal decomposition or hydrolysis of pigmented particles, special studies are required to evaluate the values of pressure and temperature jumps.

We believe that one of the possible mechanisms of 'multi-pulse' bleaching of a water-containing phantom is associated with the formation of microbubbles in the phantom. Under normal conditions, biological tissues and their phantoms can be considered as saturated solutions of atmospheric gases which are released as microscopic bubbles even when slightly heated. In the case of pulsed laser action, vapour-gas microbubbles are also formed near the heated particles. As a result, the thermal conductivity of the medium surrounding the absorbing particles will be significantly reduced. Thus, their maximum temperature will increase with the next pulse action. In addition, the temperature relaxation time will increase significantly. All this will lead, according to (2), to an increase in the degree of thermal destruction of dye particles, and, consequently, to a more effective bleaching of the tattooed skin phantom.

The proposed mechanism of bubble destruction of pigmented ink particles is illustrated in Fig. 9. As a result of exposure to the first laser pulses, the pigment particle is heated (Fig. 9a), at which the maximum temperature T_1 only reaches or slightly exceeds the destruction threshold. At the next

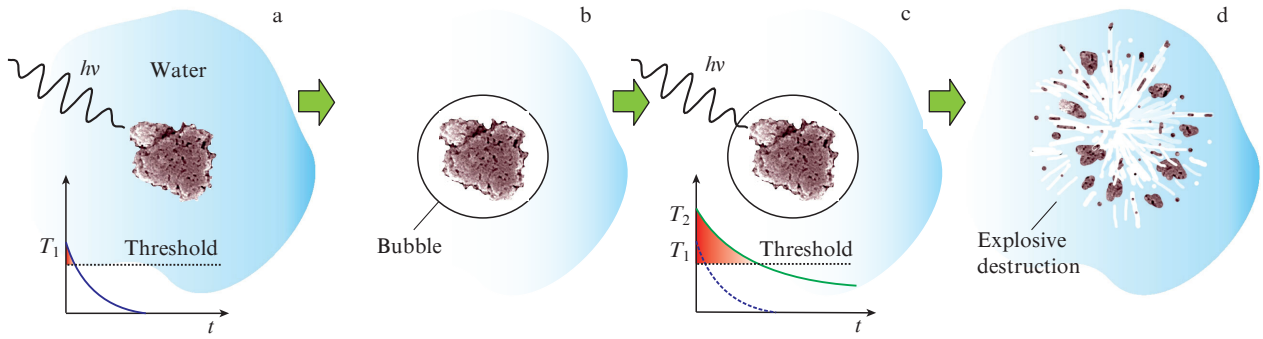

Figure 9. Assumed bubble destruction mechanism of ink particles in water: (a) heating the particle by the first laser pulse (maximum temperature T_1 slightly exceeds the destruction threshold – the particle destruction probability is small); (b) vapour-gas bubble formation due to particle heating; (c) particle heating by repeated laser pulses under conditions of its isolation by a vapour-gas bubble [maximum temperature ($T_2 > T_1$) significantly exceeds the threshold, while the relaxation time increases – the particle destruction probability is high]; (d) destruction of particles.

stage, a vapour-gas bubble is formed near the particle due to heating the water layer near the particle, which isolates the particle from the environment (Fig. 9b). Under conditions of isolation by a vapour-gas bubble, particle heating by subsequent laser pulses will be greater (Fig. 9c). The maximum temperature in this case ($T_2 > T_1$) can significantly exceed the destruction threshold. In addition, due to thermal insulation, the temperature relaxation time can also increase significantly. As a result of these two factors, the pigment destruction probability determined by (2) will increase sharply, which will lead to the particle destruction (Fig. 9d).

Since pigment agglomerates contain water, pulsed heating of such a particle to a critical temperature of $\sim T_c$ (~646.9 K) causes explosive boiling of water and the pressure inside the agglomerate abruptly increases to a pressure close to the critical value of P_c (~22.06 MPa) [26]. If the strength limit is exceeded, the impact destruction of the agglomerate and its largest nanoparticles occurs. As a result of a sharp increase in the total surface area of the formed nanoparticles, the probability of their further destruction and utilisation increases.

Another interesting effect should be taken into account in the proposed bubble mechanism of ink particle destruction. It is known [28] that vapour-gas microbubbles actively adsorb nanoparticles located in a colloid on their surface. In this regard, microbubbles formed during pulsed laser heating will effectively accumulate ink nanoparticles on their surface, forming a kind of agglomerates. Due to the increase in their effective size during pulsed laser heating, the maximum temperature of these agglomerates will be significantly higher than the temperature of individual pigment nanoparticles. As a result, this process in the multipulse regime of exposure will lead, according to (2), to an increase in the degree of destruction of ink particles.

5. Conclusions

The following main results have been obtained in this work.

1. A technology for the manufacture of tattooed skin phantoms with a thickness of 170 μm based on polyacrylamide hydrogel has been developed. The phantom contains water (from 70% to 10%), organic molecules, including collagen, and tattoo ink.

2. Using probe radiation, the dynamics of the formation and relaxation of microbubbles in tattooed skin phantoms under the impact of pulsed laser radiation has been studied. It is shown that microbubbles are formed within a few milliseconds after the laser pulse action. The lifetime of microbubbles varies from a few seconds to several hours, depending on the water content in the phantom and the fluence of 'power' laser radiation.

3. The regimes of bleaching of tattooed skin phantoms by a series of laser pulses have been found, which make it possible to considerably reduce the laser fluence and significantly increase the degree of bleaching compared to the single-pulse regime. The range of parameters (number of irradiations, laser fluence) is determined, at which a high (sufficient to block the 'power' radiation) concentration of long-lived bubbles is not formed, whereas the degree of bleaching exceeds 40%.

4. Possible mechanisms of destruction of pigmented particles contained in tattooed skin phantoms by a series of laser pulses are considered. A bubble mechanism of laser-induced bleaching based on a change in the thermal conductivity of the medium near the pigmented particle due to the formation of a vapour-gas bubble is proposed. As a result, both the maximum temperature and the temperature relaxation time increase, which increases the probability of ink particle destruction.

Acknowledgements. In part of analysing the possibility of laser formation of supercritical water, the work was supported by the Russian Foundation for Basic Research (Grant No. 18-29-06056), in part of laser transformation of pigmented titanium oxide nanoaggregates, by the Ministry of Science and Higher Education in the framework of the State Task of the Federal Research Centre 'Crystallography and Photonics' of the Russian Academy of Sciences.

References

1. Jones C.P., Gustafson M., Macquarrie C.W., Rosecrans J.A., et al., in *Written on the Body: the Tattoo in European and American History* (London: Reaktion, 2000) p. 1.
2. Taylor C.R., Anderson R.R., Gange R.W., Michaud N.A., Flotte T.J. *J. Investigat. Dermatol.*, **97**, 131 (1991).
3. Alster T., in *Manual of Cutaneous Laser Techniques* (Philadelphia: Lippincott Williams & Wilkins, 2000) p. 77.
4. Miranda M.D. *Forensic Analysis of Tattoo and Tattoo Inks* (Boca Raton: Taylor & Francis Group, 2016) p. 97.
5. Hsu V.M., Aldahan A.S., Mlacker S., Shah V.V., Nouri K. *Lasers Med. Sci.*, **31**, 17337 (2016).
6. Ganguly M., Mitra K., in *Proc.CHT-15. 6th Internation Symposiume on Advances in Computational Heat Transfer* (New Branswick, NJ, USA: Rutgers University, 2015) p. 368.

7. Naga L.I., Alster T.S. *Am. J. Clin. Dermatol.*, **18**, 59 (2017).
8. Hardy C.L., Kollipara R., Hoss E., Goldman M.P. *Lasers Surg. Med.*, **52**, 583 (2020).
9. Choi M.S., Seo H.S., Kim J.G., Choe S.J., Park B.C., Kim M.H., Hong S.P. *PloS One.*, **13**, e0203370 (2018).
10. Torbeck R.L., Schilling L., Khorasani H., Dover J.S., Arndt K.A., Saedi N. *Dermatol. Surg.*, **45**, 183 (2019).
11. Bäumler W., Weiß K.T. *Photochem. Photobiol. Sci.*, **18**, 349 (2019).
12. Belikov A.V., Shamova A.A., Shandybina G.D., Yakovlev E.B. *Quantum Electron.*, **49**, 52 (2019) [*Kvantovaya Elektron.*, **49**, 52 (2019)].
13. Kossida T., Rigopoulos D., Katsambas A., Anderson R.R. *J. Am. Acad Dermatol.*, **66**, 271 (2012).
14. Reddy K.K., Brauer J.A., Anolik R., Bernstein L., Brightman L., Hale E., Karen J., et al. *Lasers Surg. Med.*, **45**, 76 (2013).
15. Luebberding S., Alexiades-Armenakas M. *Dermatol.Clin.*, **32**, 91 (2014).
16. Vangipuram R., Hamill S.S., Friedman P.M. *Lasers Surg. Med.*, **50**, 890 (2018).
17. Manenkov A.A., Prokhorov A.M. *Usp. Fiz. Nauk*, **148** (1), 179 (1986).
18. Tobin D.J. *Chem. Soc. Rev.*, **35** (1), 52 (2006).
19. Shubnyy A.G., Zhigarkov V.S., Yusupov V.I., Sviridov A.P., Bagratashvili V.N. *Proc. SPIE*, **10716**, 1071611-1-11 (2018).
20. Kondyurin A.V., Sviridov A.P. *Quantum Electron.*, **38**, 641 (2008) [*Kvantovaya Elektron.*, **38**, 641 (2008)].
21. Ho D.D.M., London R., Zimmerman G.B., Young D.A. *Lasers Surg. Med.*, **30**, 389 (2002).
22. Zhang L., Belova V., Wang H., Dong W., Möhwald H. *Chem. Mater.*, **26**, 2244 (2014).
23. Gupta S.M., Tripathi M. *Chin. Sci. Bullet.*, **56**, 1639 (2011).
24. Wu T., Lin T., Zhao J., Hidaka H., Seprone N. *Environ. Sci. Technol.*, **33**, 1379 (1999).
25. Baffou G., Rigneault H. *Phys. Rev. B*, **84**, 035415 (2011).
26. Yusupov V.I. *Sverkhkrit. Flyuidy: Teor. Prakt.*, **14** (1), 71 (2019).
27. Cocero M.J. *J. Supercrit. Fluids*, **134**, 124 (2018).
28. Yusupov V.I., Tsypina S.I., Bagratashvili V.N. *Laser Phys. Lett.*, **11**, 116001 (2014).